https://doi.org/10.5194/egusphere-2026-1947
Preprint. Discussion started: 27 April 2026

Present and future responses of near-surface wind speed to different land-use and land-cover types in China

Hui-Shuang Yuan[1], Yang Xu[1], Zhi-Da Sun[1], Zi-Han Wang[1], Youli Chang[1, *], Cheng Shen[2, *]

[1]Department of Atmospheric Science, Yunnan University, Kunming, China.
[2]Department of Earth Sciences, University of Gothenburg, Gothenburg, Sweden.

Correspondence to: Cheng Shen (cheng.shen@gu.se); Youli Chang (ylchang@ynu.edu.cn)

Abstract. Near-surface wind speed (NSWS) is highly sensitive to land-use and land-cover change (LULCC). However, previous studies have mainly focused on overall LULCC effects, leaving the attribution of wind variations to individual land transitions and management poorly constrained. Here, we utilize simulations from the latest land-use model intercomparison project (LUMIP) in CMIP6 to disentangle and quantify the responses of NSWS to different LULCC types over China from 1970 to 2014. We find that the primary-to-grazing transition is the dominant factor to LULCC-Induced NSWS variability, followed by fertilizer use, with urbanization contributes the least among the examined types. Future projections further suggest that land-use pathways can substantially perturb wind patterns, with low-emission pathways under minimally regulated land use producing more pronounced alterations than high-emission pathways under sustainable land use. These results highlighting the importance of resolving LULCC in attributing and projecting NSWS changes, with implications for climate modeling, wind-energy assessment, and land-use policy.

1 Introduction

Near-surface wind speed (NSWS), typically measured at 10 meters above the ground, is a critical variable influencing atmospheric processes and environmental systems (Zha et al., 2016). NSWS is vital for understanding climate variability as it affects the evaporation of surface water and thus influences the water cycle (Dunn et al., 2022; Minola et al., 2023). Furthermore, NSWS is essential for supporting renewable energy development, acting as the direct source of wind power needed to mitigate climate change (Pryor & Barthelmie, 2021; Zha et al., 2021a; Shen et al., 2024). In recent four decades, a widespread decline in NSWS, referred to as "stilling", was observed across more than 70% of mid-latitude land stations in the Northern Hemisphere between the 1980s and 2010s (Vautard et al., 2010; Yan et al., 2026). Similar phenomena are also observed in China, where with the largest reduction occurring in spring and the largest increase occurring in autumn, raising concerns about its future evolution and underlying causes (Yang et al., 2021; Zha et al., 2021b). Although land NSWS has declined, marine NSWS increased before 2010 (Zheng et al., 2016), highlighting the key role of surface modifications in global land stilling. Reanalysis datasets, which are considered to have limited sensitivity to LULCC effects, generally fail to replicate

https://doi.org/10.5194/egusphere-2026-1947
Preprint. Discussion started: 27 April 2026

this observed slowdown, suggesting the need to better incorporate surface roughness into weather and climate models (Vautard et al., 2010; Zeng et al., 2019).

Previous attributions of LULCC-Induced NSWS changes have largely relied on a limited number of land-use processes, which may have hindered a deeper understanding of the role of LULCC. For instance, existing studies have largely linked these NSWS changes to urbanization, based on comparisons between urban and rural meteorological measurements (Li et al., 2017; Wang et al., 2020). However, inconsistencies in the definitions of urban and rural, alongside variations in methodological approaches, have introduced significant uncertainties (Li et al., 2008). Using high-resolution aerodynamic roughness length data, recent studies estimate that urbanization accounts for approximately 11% of the observed NSWS reductions in China, with the most significant impacts occurring in southeastern China (Zhang et al., 2019). Although such studies support the importance of surface roughness changes for NSWS, it remains challenging to determine whether these modifications are strictly driven by urbanization. Other concurrent LULCC processes, including the transition of natural land to managed pastures and widespread fertilizer application, modify not only surface friction but also boundary-layer stability, implying that the non-urban drivers of NSWS variations might be vastly underestimated (Christidis et al., 2013; Tran et al., 2017; Sierra et al., 2021; Wu et al., 2025; Zhang et al., 2025).

Despite this complexity, quantitative assessments of individual LULCC types focus predominantly on urbanization, and analyses of other processes, such as land-state transitions and land-management practices, remain scarce (Shen et al., 2021; Liu et al., 2024). In addition, different vegetation and land-cover types can influence NSWS through multiple complex pathways. Previous studies have focused on aerodynamic roughness, whereas other physical pathways, such as local temperature changes and near-surface circulation variations driven by surface albedo, have received much less attention (Zha et al., 2021c; Wang et al., 2024; Wang et al., 2025). As a result, the specific responses of NSWS to distinct types of land-cover change remain poorly constrained. Moreover, the future implications of LULCC under different emission scenarios have also received limited attention, leaving substantial gaps in our understanding of projected NSWS changes.

To address these gaps, we employ the Land-Use Model Intercomparison Project (LUMIP) form land-use forcing using Coupled Model Intercomparison Project Phase 6 (CMIP6) experiments with ridge regression to investigate the effects of LULCC on NSWS over China during 1970–2014, quantify the contributions of individual LULCC types, including land-use transitions and management practices, and assess the impacts of future LULCC on NSWS. The remainder of this paper is structured as follows: Section 2 details the data sources and methods. Section 3 presents the results. Section 4 summarizes the main conclusions and discusses the implications for climate modeling, renewable energy planning, and land management.

https://doi.org/10.5194/egusphere-2026-1947
Preprint. Discussion started: 27 April 2026

2 Materials and Methods

2.1 Global climate models

To quantify the impact of LULCC on NSWS, we employed simulations from the LUMIP, part of the CMIP6 (O'Neill et al., 2016). The LUMIP is an endorsed CMIP6 activity that provides targeted experiments to quantify the impacts of Land states and management on climate (Lawrence et al., 2016). In CMIP6, the standard historical experiment includes all anthropogenic and natural forcings, with prescribed LULCC. LUMIP adds a complementary experiment, hist-noLu, in which land-use and management are fixed at 1850 levels. Comparing CMIP6 historical experiments with LUMIP hist-noLu help to isolates the contribution of LULCC to NSWS (Santos et al., 2023).

For future projections, we analyzed two land-use shared socioeconomic pathways (SSPs): SSP126 and SSP370. SSP126 represents a low-emission pathway with sustainable land-use managements, and SSP370 depicts a high-emission pathway with extensive land-use expansion (Ito & Hajima, 2020). Additional sensitivity experiments ("SSP126-SSP370Lu" and "SSP370-SSP126Lu") swapped land-use datasets between the two scenarios to isolate the effects of varying land-use intensities under contrasting emission pathways (Tang et al., 2023). Comparing these experiments with their parent scenarios (SSP126 and SSP370, respectively) quantifies how NSWS would change in futures in which only land-use policy is altered, which can indicate the potential impacts of LULCC in future. Details of these scenarios are presented in Table 1. All model outputs were bilinearly interpolated onto a 1° × 1° grid, and annual means were used. Details of the model experiments used are provided in Table 2.

Table 1. Used experiment of CMIP6.

Experiment name	Experiment Forcings	Experiment Description
historical	Historical with all forcings	CMIP6 historical simulation
hist-noLu	Historical with all forcings except for LULCC	CMIP6 historical simulation
ssp126	Projection with SSP1-2.6 scenario	CMIP6 low forcing scenario projection based on SSP1-2.6
ssp126_ssp370Lu	SSP1-2.6 with SSP3-7.0 land use	Same as ssp126 except for use of SSP3-7.0 land use scenario
ssp370	Projection with SSP3-7.0 scenario	CMIP6 high forcing scenario projection based on SSP3-7.0
ssp370_ssp126Lu	SSP3-7.0 with SSP1-2.6 land use	Same as ssp370 except for use of SSP1-2.6 land use scenario

https://doi.org/10.5194/egusphere-2026-1947
Preprint. Discussion started: 27 April 2026

78 **Table 2. Used model of CMIP6.**

Model	Ensemble Member	Institution	Resolution (lat*lon)
ACCESS-ESM1-5	10	Commonwealth Scientific and Industrial Research Organisation, Australia	145*192
BCC-CSM2-MR	1	Beijing Climate Center, China	160*320
CanESM5	10	Canadian Centre for Climate Modelling and Analysis, Canada	64*128
CMCC-ESM2	1	Fondazione Centro Euro-Mediterraneo sui Cambiamenti Climatici, Italy	192*288
IPSL-CM6A-LR	4	Institut Pierre Simon Laplace, France	143*144
MIROC-ES2L	1	Japan Agency for Marine-Earth Science and Technology,Atmosphere and Ocean Research Institute,The University of Tokyo,National Institute for Environmental Studies,RIKEN Center for Computational Science, Japan	64*128
MPI-ESM1-2-LR	1	Max Planck Institute for Meteorology, Germany	96*192
NorESM2-LM	1	NorESM Climate modeling Consortium, Norway	96*144
UKESM1-0-LL	4	Met Office Hadley Centre, UK	144*192

79

80 **2.2 Gridded observational data**

81 The monthly CN05.1 dataset (Wu & Gao, 2013), with a spatial resolution of 0.25°×0.25°, serves as a reliable reference for
82 assessing observed NSWS variations and benchmarking model simulations (Cheng Shen et al., 2022; Chuan et al., 2024; Li et
83 al., 2024; Zha et al., 2024; Li et al., 2025). In this paper, it was interpolated into 1°×1°, and employed to validate the
84 performance of global climate models in simulating NSWS changes over China from 1970 to 2014 (Wu et al., 2017; Long et
85 al., 2021). It also served as the target for ridge regression and as the reference for assessing that method's effectiveness in
86 correcting the models (Sect. 2.5).

87 **2.3 Land-use harmonization dataset**

88 We employed the Land-Use Harmonization 2 (LUH2) dataset, a global gridded dataset designed for climate modeling, to
89 analyze the roles of LULCC in shaping NSWS (Hurtt et al., 2020). The LUH2 dataset provides annual data at 0.25° × 0.25°

https://doi.org/10.5194/egusphere-2026-1947
Preprint. Discussion started: 27 April 2026

resolution, incorporating updated inputs, and detailed representations of land-use states, transitions and agricultural management (Hurtt et al., 2020; Chini et al., 2021). For this study, LUH2 data during 1970 to 2014 were selected. To ensure compatibility with other datasets and models, all fields were interpolated to a 1°×1° grid. The dataset is provided in three LULCC types: states, transitions, and management. In LUH2, land cover is divided into 12 types (Hurtt et al., 2020). For each grid cell, land-use states are provided as area fractions and transitions as annual conversion areas, allowing multiple land-use types to coexist within the same grid cell. To obtain more interpretable results and to avoid overparameterization in the ridge regression, we merge these into five broad categories. The merging scheme is informed by Hurtt et al. (2020), with the specific mapping given in Table 3.

Table 3. LUH2 state-type aggregation scheme and management categories.

State	
Cropland	C3 annual crops (c3ann), C3 nitrogen-fixing crops (c3nfx), C3 perennial crops (c3per), C4 annual crops (c4ann), C4 perennial crops (c4per)
Grazing	managed pasture (pastr), rangeland (range)
Primary	forested primary land (primf), non-forested primary land (primn)
Secondary	potentially forested secondary land (secdf), potentially non-forested secondary land (secdn)
Urban	urban land
Management	
Fertl	fertilization
Irrig	irrigation

The variables of state and management represent, for each year, the land-use composition and management intensity in each grid cell. In contrast, transition records year-to-year flows between land-use types, i.e., the change from one year to the next (records labeled with a given year refer to the change between that year and the following year). To pair land-use change with NSWS for a given year, we sum transitions through the previous year so that the cumulative land-use change history aligns with the state, management, and LULCC-Induced NSWS for that year.

2.4 Impact of LULCC on NSWS

The historical and hist-noLu experiments from LUMIP provide a controlled framework to isolate the contribution of LULCC to NSWS, which is difficult to disentangle using observations alone. The historical simulations incorporated observed LULCC,

https://doi.org/10.5194/egusphere-2026-1947
Preprint. Discussion started: 27 April 2026

including land-use transitions and management practices, whereas land use in "hist-noLu" is fixed at its 1850 level. Therefore, the changes of NSWS caused by LULCC could be calculated as:

$$NSWS_{\text{LULCC-induced}} = NSWS_{\text{historical}} - NSWS_{\text{hist-nolu}}, \quad (1)$$

For future, we analyze the LUMIP experiments SSP126-SSP370Lu and SSP370-SSP126Lu, which replace each scenario's background with the other scenario's LULCC forcing. The former keeps all forcings other than land use from SSP126 and substitutes the SSP370 land-use forcing (LUH2 states, transitions, management, and harvest); the latter keeps the SSP370 background and substitutes the SSP126 land-use forcing. Comparing each swap with its parent scenario yields an estimate of the land-use contribution to NSWS under both low- and high-emissions backgrounds, probing interactions between emissions and land use. Finally, the difference between SSP126-SSP370Lu and SSP126 quantifies the effect of adopting an intensive land-use pathway within a low-emissions background. In contrast, the difference between SSP370-SSP126Lu and SSP126 quantifies the effect of adopting a sustainable pathway within a high-emissions background. Together, these contrasts indicate the potential impact and importance of LULCC for future NSWS.

2.5 Ridge regression analysis

To reduce uncertainty from model deficiencies, we applied ridge regression to calibrate model contributions based on their skill in reproducing historical NSWS changes (Hoerl & Kennard, 1970). Within this workflow, all variables were standardized to ensure comparability across units and scales. The ridge penalty shrinks large coefficients, mitigates multicollinearity, and yields a balanced integration that avoids overemphasizing any single model (Tebaldi & Knutti, 2007). The historical simulations of individual models were used as independent variables, while observational data served as the dependent variable. The relationship can be described as Eq. (2):

$$NSWS_{\text{obs}} = \sum R_i M_i + Res, \quad (2)$$

where NSWS_{obs} represents the reference, which is the CN05.1 dataset in this study. M_i denotes the standardized historical experiment series from the model. Ri is the corresponding regression coefficient. When calibrating the models, to ensure the ridge regression-based information is a valid rather than spurious signal (i.e., to avoid negative correlations between observations and model predictors), all Ri are constrained to be non-negative.

2.6 Contributions of Various LULCC Types

We also apply ridge regression to quantify the contributions of land states and transitions on NSWS, leaving coefficient signs unconstrained since negative associations can be reasonable. Different land use types and transitions describe related aspects of land surface change and may therefore introduce multicollinearity, which can destabilize conventional regression estimates and hinder the attribution of individual contributions. Ridge regression was used to address this issue by applying a penalty term that shrinks the coefficients of correlated predictors and stabilizes their estimates. All variables were standardized before

https://doi.org/10.5194/egusphere-2026-1947
Preprint. Discussion started: 27 April 2026

model fitting to ensure that predictors with smaller magnitudes, such as those related to urban land use, were not assigned disproportionately small coefficients because of differences in scale. The way to quantify effects of different LULCC on NSWS can be divided into two steps. Specifically, we posit that the LULCC-driven component of NSWS depends on land states and management. Different land states and management practices in LUH2 may be associated with different expected wind speeds. Accordingly, we approximate this dependence with ridge regression that links land-state and management indicators to the LULCC-Induced NSWS following Eq. (3):

$$\Delta NSWS = \sum_{k \in S} R_k X_k + Res, \tag{3}$$

Here, the index set S includes five land states and two management practices (cropland, grazing, primary, secondary, urban; fertilization and irrigation). X represents the area land state, or irrigated area and the total nitrogen fertilizer rate across all crop types, for 1970–2014. The relative contribution of each explanatory variable to LULCC-Induced variability was calculated following Eq. (4):

$$RC = \frac{|R_i|}{\sum_i |R_i|}, \tag{4}$$

where $|R_i|$ is the absolute value of the relative contribution of its explanatory variable. This approach, grounded in regression coefficient analysis, allows for clearer interpretation of the proportional impact of each variable within the model (Bring, 1994; Grömping, 2007). This analysis enabled clear interpretation of the proportional impact of each variable, identifying dominant LULCC types driving NSWS changes across China.

For each land state, we interpret the corresponding linear term from step 1 as a proxy for the portion of LULCC-Induced NSWS associated with that state. This state-level contribution is then further attributed to specific transition types and, where applicable, harvest. Therefore, we employ the ridge regression again to link the contribution of specific land states and relevant transitions and harvest following Eq. (5):

$$R_{\text{state A}} X_{\text{state A}} = \sum_{i \in S(\text{state A})} R_i Y_i + Res, \tag{5}$$

The relative contribution of a given term is computed as:

$$RC_{\text{state A to state B}} = \frac{|R_{\text{states A to state B}}|}{\sum_{i \in S(\text{state A})} |R_i|} RC_{state\ A} + \frac{|R_{\text{states A to state B}}|}{\sum_{j \in S(\text{state B})} |R_j|} RC_{\text{state B}}, \tag{6}$$

$$RC_{\text{harvest of state A}} = \frac{|R_{\text{harvest of state A}}|}{\sum_{i \in S(\text{state A})} |R_i|} RC_{\text{state A}}, \tag{7}$$

Here Y_i denotes the transition or harvest. RC_{state} denotes the state-level relative contribution. $RC_{\text{state A to state B}}$ denotes the estimated relative contribution of that transition to the variability of LULCC-Induced NSWS, and $RC_{\text{harvest of state A}}$ denotes the estimated relative contribution for the harvest of that state (if present). The index sets S (state A) and S (state B) collect the variables relevant to each state, namely all incoming and outgoing transitions involving that state and, for states with harvest, the harvest term. Table 4 provides details for the variable each state includes. Thus, the relative contributions sum to 1 for both individual grid cells and the area mean.

https://doi.org/10.5194/egusphere-2026-1947
Preprint. Discussion started: 27 April 2026

Table 4. The variable that each state relevant.

State	
Cropland	cropland to grazing; cropland to secondary; cropland to urban; grazing to cropland; primary to cropland; secondary to cropland; urban to cropland
Grazing	grazing to cropland; grazing to secondary; grazing to urban cropland to grazing; primary to grazing; secondary to grazing; urban to grazing
Primary	primary to cropland; primary to grazing; primary to secondary; primary to urban; primary harvest
Secondary	secondary to cropland; secondary to grazing; secondary to urban; secondary harvest cropland to secondary; grazing to secondary; primary to secondary; urban to secondary
Urban	urban to cropland; urban to grazing; urban to secondary; cropland to urban; grazing to urban; primary to urban; secondary to urban

The sign of the association between a given transition or harvest and LULCC-Induced NSWS is determined by the sign of the ridge regression coefficient (positive indicates a positive correlation). However, this sign information is lost when computing the relative contribution in Eq. (6). To retain it, we also employ a sign-preserving formulation of the relative contribution, defined following Eq. (8):

$$RC_{\text{state A to state B}} = \frac{R_{\text{states A to state B}}}{\sum_{i \in S(\text{state A})} |R_i|} RC_{\text{state A}} + \frac{R_{\text{states A to state B}}}{\sum_{j \in S(\text{state B})} |R_j|} RC_{\text{state B}}, \quad (8)$$

This method does not enforce that relative contributions sum to 1 and is used solely to display the correlation sign. The resulting relative contributions may differ slightly from those of the previous method, yet their magnitudes still indicate how strongly a given transition or harvest contributes to LULCC-Induced NSWS variability at a given location.

2.7 Model evaluation

The performance of each model on NSWS simulation was evaluated over 1970–2014 using correlation coefficients, modeled-to-observed trend ratios, root-mean-square error (RMSE), and Skill scores (Shen et al., 2021; C. Shen et al., 2022; Yuan et al., 2025). All metrics were computed from the spatially averaged NSWS time series over China, with the Tibetan Plateau masked out. The Skill score is calculated using the following equation:

$$Skill\ score = \frac{(1+CC)^2}{(SDR+\frac{1}{SDR})^2}, \quad (9)$$

where CC refers to the correlation coefficient, and SDR refers to the standard deviation ratio between the observation and simulation.

https://doi.org/10.5194/egusphere-2026-1947
Preprint. Discussion started: 27 April 2026

3 Results

3.1 LULCC-Induced NSWS Changes

We first examine the performance of individual models and the conventional multi-model ensemble (MME) in simulating observed NSWS over China. Figure 1a–d shows that the original outputs of LUMIP models struggle to simulate observed NSWS over China, even for spatially averaged time series. Correlation coefficients between observations and models are generally below 0.5 and even fail to reach statistical significance, except for UKESM1-0-LL (Fig. 1a). Across models, NSWS trends are substantially underestimated, with simulated trends are generally one tenth of the observed trend or less (Fig. 1b). RMSEs are comparable across models at about 0.25 m s^{-1} (roughly 10% of the observed mean of 2.56 m s^{-1}), suggesting the mean state is reasonably captured (Fig. 1c). Meanwhile, skill scores for both individual models and the MME are generally below 0.1, indicating limited skill (Fig. 1d). In general, individual models perform poorly in terms of correlation, trend magnitude, and the overall skill score, whereas mean NSWS is reproduced well. Moreover, the MME offers no clear advantage.

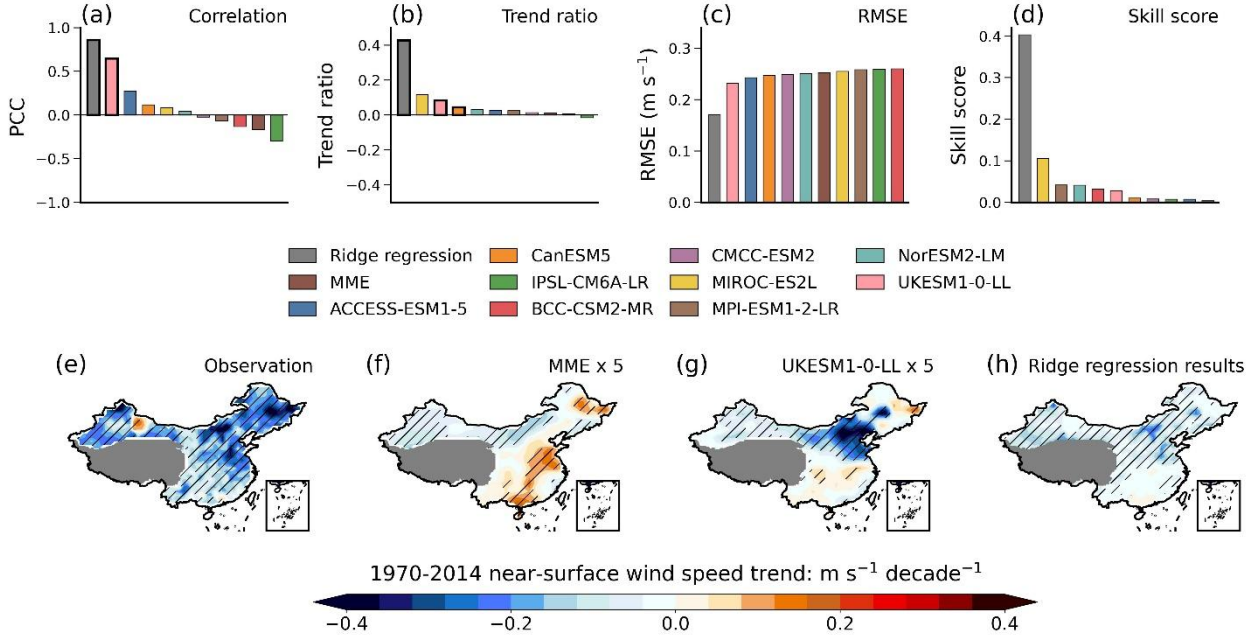

Figure 1: Evaluation of the ability of LUMIP models in simulating NSWS and spatial distribution of NSWS trends (m s-1 decade-1) over China during 1970–2014. Panels (a)–(d) report the correlation coefficient, the modeled-to-observed trend ratio relative to the CN05.1 observational dataset, the RMSE, and the Skill score for spatially averaged NSWS time series over China (with Tibetan Plateau masked). Black bold bars indicate correlations significant at the 99% confidence level in (a) and trends significant at the 99% confidence level in (b). Panels (e)–(h) show observation, MME, UKESM1-0-LL, and ridge regression, respectively. Hatching indicates the trend is statistically significant at the 0.01 level. The MME and UKESM1-0-LL trends are relatively small; for comparability, panels (f) and (g) show trends scaled by ×5.

Although individual models generally perform poorly, their results differ, and some perform better in specific aspects, possibly owing to a more realistic treatment of factors affecting NSWS, such as LULCC. Among individual models, UKESM1-0-LL

https://doi.org/10.5194/egusphere-2026-1947
Preprint. Discussion started: 27 April 2026

performs best, exhibiting a statistically significant correlation coefficient and trend while attaining the smallest RMSE. To gain more insight into the ability in models to simulate NSWS trends, we further compare the spatial distribution of NSWS trends over China among observations, the MME, and UKESM1-0-LL. Observations show a widespread decline in NSWS across China (Fig. 1e). However, neither the MME nor UKESM1-0-LL reproduces this broad weakening, especially over northern China, and their trend magnitudes are much smaller than observation (Fig. 1f–g). Notably, the MME shows significant increasing trends in some regions, which is a problem much less evident in UKESM1-0-LL. This indicates that the MME provides limited improvement over the individual models (Fig. 1f). This limitation may stem from the generally weak skill of the constituent models. Equal-weight averaging likely dilutes the signal and propagates inaccuracies, offsetting potential gains (Fig. 1a–d).

In contrast, by assigning greater weight to models with higher skill, ridge regression can help mitigate the limitations of equal-weight averaging. Ridge regression model performs better across all nationally averaged NSWS metrics and spatial trend patterns for 1970–2014, outperforming both individual models and the multi-model ensemble. The pattern correlation coefficient is 0.86 ($P<0.01$). Although ridge regression still underestimates the mean trend (the trend ratio is around 0.4, meaning roughly 40 percent of the observed trend), its improvement over individual models and the equal-weight ensemble is substantial, with the RMSE is less than 0.20 m s^{-1}. Considering correlation together with the standard-deviation ratio, the composite skill score is higher (around 0.4). For spatial patterns, ridge regression shows clear improvement, avoiding spurious increases over South China and yielding trend magnitudes closer to observations. Overall, it provides consistent gains in both mean metrics and spatial realism, offering a more reliable reconstruction than either individual models or the ensemble. It also implies that credible LULCC attribution requires reliable skill.

https://doi.org/10.5194/egusphere-2026-1947
Preprint. Discussion started: 27 April 2026

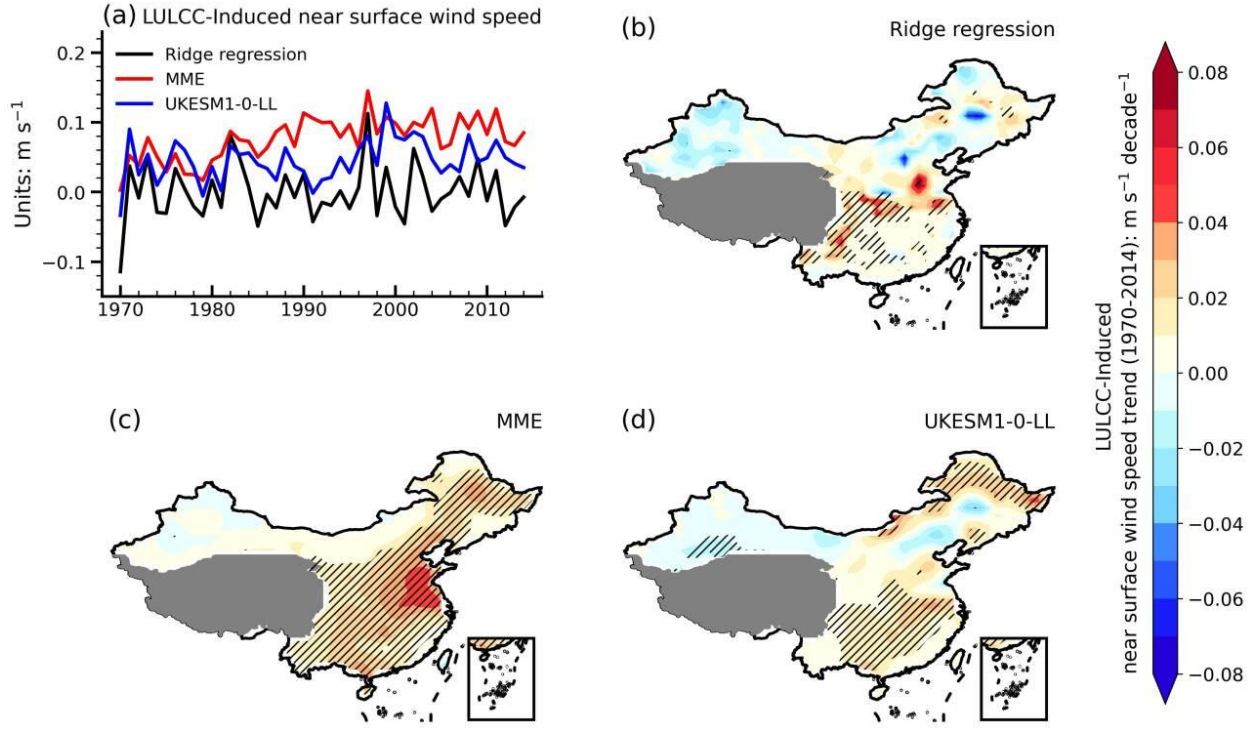

Figure 2: Averaged annual-mean and spatial trend patterns of LULCC-Induced NSWS over China during 1970–2014. (a) Averaged annual mean time series of LULCC-Induced NSWS over China during 1970–2014 for ridge regression, MME and UKESM1-0-LL. Spatial trend patterns of LULCC-Induced NSWS over China during 1970–2014 for (b) ridge regression, (c) MME and (d) UKESM1-0-LL. Hatching indicates the trend statistically significant at the 0.01 level.

Given the superior performance of ridge regression relative to the MME and any single model, we therefore employ it to derive the historical LULCC-Induced NSWS signals. Using coefficients derived by regressing historical simulations on observations, we bias-correct hist-noLu and benchmark it against historical, defined as historical minus hist-noLu (Sect. 2.4). Figure 2 shows the LULCC-Induced NSWS changes derived from ridge regression, alongside results from the MME and UKESM1-0-LL. According to ridge regression, from a national scale, the averaged NSWS time series over China (excluding the Tibetan Plateau) exhibits no significant trend (Fig. 2a). The corresponding spatial pattern of NSWS trends shows a statistically significant increase in southern China, whereas the decrease in northern China is not significant (Fig. 2b). The ridge regression model estimate agrees more closely with UKESM1-0-LL than with the MME, suggesting that the correction relies more on models whose behavior better matches observations (Fig. 2b, d and f). Compared with the ridge regression results, both the MME and UKESM1-0-LL exhibit spurious, widespread LULCC-Induced increases in NSWS (Fig. 2c–f). This likely stems from suboptimal historical performance, as similar spurious increases are evident relative to observations.

https://doi.org/10.5194/egusphere-2026-1947
Preprint. Discussion started: 27 April 2026

3.2 Relative contributions of LULCC types

We further attribute LULCC-Induced NSWS to individual LULCC types. We assume that, with other forcings and factors held constant, regional NSWS variation depends on surface conditions, namely state and management. The same also holds for their changes. In other words, different states and management roughly correspond to different ranges of NSWS, so changes in land-state composition and management lead to NSWS changes. Specifically, we treat these as the independent types associated with LULCC-Induced NSWS. Figure 3 shows the relative contributions of individual land states and management practices to NSWS variability in China during 1970–2014. In the attribution based on land-state and land-management variables, contributions from different states and management are comparable in magnitude, indicating that NSWS changes arise from many factors (Fig. 3a). Among them, grazing contributes the most, followed by secondary land. Comparatively, the variability associated with urban change is the smallest among the five land states and two management practices, likely because LUH2 shows very limited urban extent at the national scale, as the national mean urban fraction was only around 0.5% during 1970–2015, whereas grazing covers about 28% and secondary vegetation about 21%. Many regions in China contain no urban land at all. Hence, when averaging nationally, it is reasonable that urban contributes the least to variability.

https://doi.org/10.5194/egusphere-2026-1947
Preprint. Discussion started: 27 April 2026

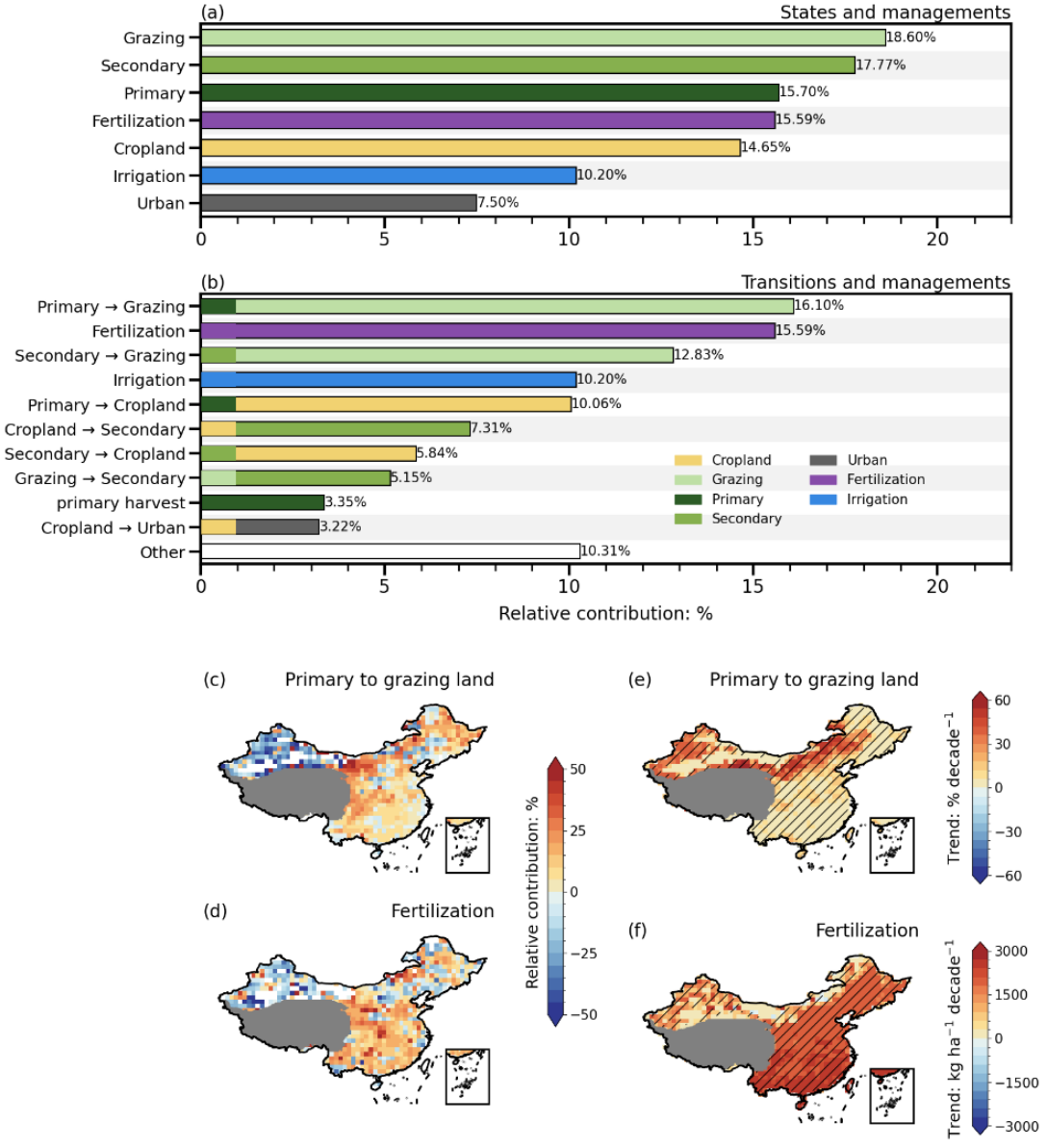

Figure 3: Relative contributions of LULCC types to LULCC-Induced NSWS changes over China, and the spatial patterns and trends of contributions from the primary-to-grazing transition and fertilization. (a) Contributions by land states and management. (b) Contributions by transitions and management. The relative contribution of states was estimated using ridge regression between LULCC-Induced changes and state and management variables; the transition contribution was then derived from these state-based contributions. In each horizontal bar except harvest, the left segment indicates the origin land states, and the right segment indicates the destination land states. Only the top ten transitions or harvest categories with the largest relative contributions are shown. (c-d): Spatial patterns of the relative contributions of the (c) primary-to-grazing transition and (d) fertilization. (e-f): Spatial patterns of the trend of the (e) primary-to-grazing transition and (f) fertilization.

https://doi.org/10.5194/egusphere-2026-1947
Preprint. Discussion started: 27 April 2026

Changes in a LULCC state do not occur in isolation. In general, they arise from land transitions involving at least one other state. The results from the first step quantify the importance of each state for NSWS on its own, whereas the results from the second step identify which transitions contribute most to NSWS changes and focus the analysis on land change processes, which better aligns with intuition. Furthermore, we decompose the contribution of each state into specific transitions. The expansion of grazing land (mainly from primary land and secondarily from secondary land) makes a substantial contribution to LULCC-Induced NSWS variability, accounting for 28.93%, in all transition types. Among urban land changes, only the crop-to-urban transition ranks among the top ten contributors, indicating that rapid, cropland-consuming urbanization does affect NSWS (Fig. 3b). However, due to its small spatial footprint, urbanization remains a modest contributor to the national average.

Figure 3 also illustrates that the same land-use transition or management practice can lead to distinct NSWS responses across regions, supporting the complex nature of LULCC impacts in China. Overall, the transition from primary land to grazing land emerges as the dominant contributor to LULCC-Induced increases in NSWS, and ridge regression attribution for 1970–2014 further confirms this, as a positive contribution is more general (Fig. 3c). This transition happens mainly in Inner Mongolia, northern China, where intensive livestock production and the arid to semiarid climate favor pasture expansion (Fig. 3e). Mechanistically, relative to grazing land, primary land might support more diverse and structurally complex vegetation, yielding greater surface roughness; replacing it with grazing land reduces roughness and can enhance NSWS. Consequently, the decline in primary land together with the expansion of grazing land, which might reflect growth of the livestock sector, likely contributed to the observed rise in NSWS over China in recent decades.

Following the primary-to-grazing transition, fertilization acts as the second largest positive driver of LULCC-Induced NSWS changes (Fig. 3b). Between the two examined management practices, fertilization exerts a substantially stronger impact than irrigation, as fertilization explains ~16% of LULCC-Induced NSWS variability, compared with ~10% for irrigation. Mechanistically, fertilization stimulates vegetation growth and canopy closure, which would be expected to increase aerodynamic roughness and perturb near-surface flow. Concomitant increases in vegetation cover may also modify surface albedo and evapotranspiration, thereby affecting boundary-layer stability and local winds. Accordingly, the net NSWS response to fertilization is plausibly bidirectional. In our results, increases in fertilization are associated with NSWS enhancement across much of China, except in northwestern China. This suggests that the positive effect, on balance, is more common (Fig. 3d and f).

3.3 Projected LULCC-Induced NSWS

Understanding the projected responses of NSWS to future LULCC is crucial for long-term wind-energy planning and climate mitigation. We employ a ridge regression model calibrated on historical experiments to project LULCC-Induced NSWS changes under two contrasting emissions scenarios: SSP126 (lower emissions) and SSP370 (higher emissions). These scenarios incorporate inherently divergent land-use trajectories. SSP126 emphasizes sustainable land management with

https://doi.org/10.5194/egusphere-2026-1947
Preprint. Discussion started: 27 April 2026

extensive reforestation and constrained agricultural expansion, whereas SSP370 assumes minimal environmental regulation, leading to substantial cropland and pasture expansion at the expense of forests (Popp et al., 2017).

To isolate the specific influence of these land-use trajectories from the greenhouse gas forcing, we leverage the factorial design of the LUMIP future projections. Specifically, we apply the minimal-regulation land-management setting within the SSP126 forcing background, or in contrast, sustainable land management within the SSP370 forcing background. This cross-pairing allows us to rigorously test the sensitivity of future NSWS to extreme LULCC shifts under different global warming trajectories. One scenario follows a sustainable pathway while neglecting LULCC trajectories (SSP126_SSP370Lu), whereas the other conversely focuses exclusively on them (SSP370_SSP126Lu).

By comparing these scenarios with the originals, the divergence serves to test whether LULCC trajectories alone could dominate future NSWS changes. As illustrated in Fig. 4, the divergence between SSP126_SSP370Lu and SSP126 is substantially larger than that between SSP370_SSP126Lu and SSP370. This pattern suggests that, the potential effects of minimal-regulation land-use trajectories on NSWS under low emission scenarios are more pronounced than those of sustainable land-use trajectories under high emission scenarios. Under SSP126, minimal-regulation trajectories are projected to amplify regional NSWS increases, especially in western China (Fig. 4a–c). In this setting, relatively low greenhouse gas (GHG) forcing likely heightens the sensitivity of NSWS to land management, underscoring the necessity for well-designed, sustainable land-use policies to mitigate climate impacts (Lawrence et al., 2016). Under SSP370, sustainable trajectories tend to decrease NSWS over southern China and increase it over northeast China, but the overall signal is small (Fig. 4d–f). A plausible explanation is that the dominant influence of high GHG emissions overwhelms LULCC effects, with atmospheric changes that caused by warming largely governing NSWS. Together, these results emphasize the need to integrate land-use policy with emissions-mitigation strategies to optimize wind resource availability and strengthen ecosystem resilience in a changing climate. Moreover, the divergence across periods is modest, which might indicate that the LULCC impact is approximately constant under the same forcing.

https://doi.org/10.5194/egusphere-2026-1947
Preprint. Discussion started: 27 April 2026

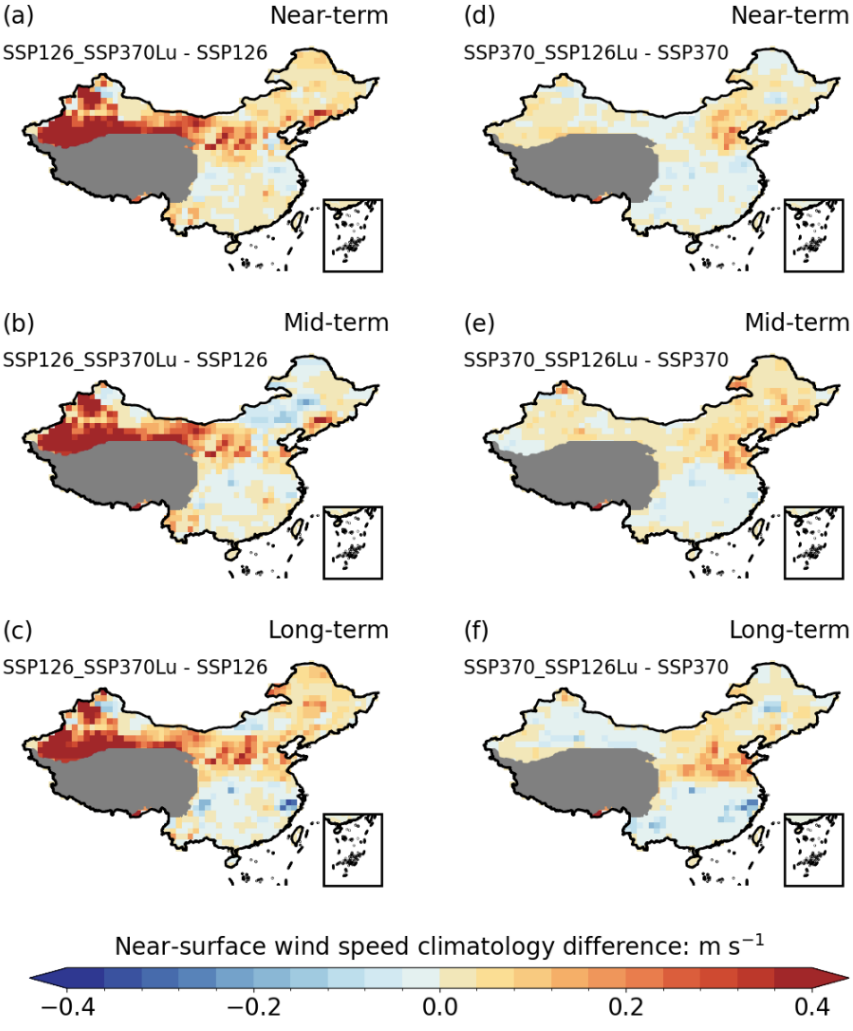

Figure 4: Future LULCC-Induced NSWS changes. (a–c) climatological near-surface wind speed (NSWS) from SSP126-SSP370Lu minus that from SSP126 for the (a) near term (2020–2040), (b) mid-term (2040–2060), and (c) long term (2080–2100); (d–f) as in (a–c) but for SSP370 minus SSP370-SSP126Lu. SSP126, SSP370, SSP126-SSP370Lu, and SSP370-SSP126Lu denote different experimental designs.

4 Discussion and conclusions

Our study employs a comprehensive evaluation of LULCC-driven NSWS across China during 1970–2014, revealing an overall positive contribution from LULCC. This overarching positive effect contrasts sharply with prevailing assumptions in the NSWS community, which have traditionally linked LULCC primarily to widespread wind stilling. Meanwhile, our results align with prior studies in demonstrating that urbanization specifically induces localized NSWS reductions, we find that this

https://doi.org/10.5194/egusphere-2026-1947
Preprint. Discussion started: 27 April 2026

decelerating effect is heavily outweighed by the two most influential positive drivers, the primary-to-grazing transition and widespread fertilizer use. Furthermore, in future scenarios, the potential influence of LULCC on NSWS is substantially more pronounced under low-emission backgrounds than under high-emission extremes. Accurately capturing its net climatic impact fundamentally requires disentangling the distinct, and sometimes opposing, roles of specific land-use transitions and management practices.

Differences in how CMIP6 models parameterize land-surface processes fundamentally drive the inter-model spread identified in this study. The mathematical and physical treatment of LULCC alters vegetation properties, surface roughness, soil moisture, and surface energy partitioning, thereby influencing sensible heating, boundary-layer development, and ultimately near-surface momentum. In this context, the superior performance of specific models, such as UKESM1-0-LL, stems from a more realistic and interactive representation of land-atmosphere coupling, such as dynamic vegetation responses and intricate canopy radiation schemes. This mechanistic advantage elucidates the efficacy of our ridge regression approach, which appropriately assigns greater statistical weight to models exhibiting higher physical skill. Nevertheless, our LUMIP-based framework provides a robust perspective on the relative contributions of individual LULCC types, the absolute magnitudes of these estimates carry uncertainties tied to the base parameterizations in models.

Previous studies argued that LULCC contributed uniformly to the historical decline of NSWS over China, our results indicate spatially heterogeneous contributions; even at the national scale, the LULCC-Induced NSWS trend is statistically neutral. Furthermore, prior observation-based attributions singled out urbanization as the dominant LULCC forcing (Zhang and Wang, 2021; Li et al., 2017), we find LULCC overarching contribution to be relatively minor, aligning well with its extremely limited areal fraction nationwide. These discrepancies are directly attributable to methodological differences. Conventional observation-minus-reanalysis approaches treat LULCC as an aggregated residual and would suffer from spatial biases due to the overrepresentation of urban meteorological stations. By utilizing controlled LUMIP experiments, our study circumvents this urban bias and demonstrates that extensive landscape transformations, rather than localized urban expansion, dictate the overall NSWS response.

The mechanisms in individual LULCC types affect NSWS remain largely unresolved. For example, our results indicate that increases in fertilization have contributed positively to NSWS across much of China, with the strongest signals in the east. A plausible mechanism is that fertilization affects NSWS mainly via local temperature and circulation changes rather than by increasing surface roughness. By contrast, irrigation appears to exert a more uniform, thermodynamically mediated influence as it cools the land surface, stabilizes soil moisture and the boundary layer, and reduces wind erosion in arid regions (Yu and Leng, 2022). These inferred mechanisms necessitate future validation using high-resolution regional climate models coupled with explicit crop-management modules.

Future work should further examine how LULCC interacts with other atmospheric variables, how its effects on NSWS vary across climatic regions, and how land-use transitions are shaped by broader socio-economic drivers. Ultimately, integrating granular land-use and land-management policies with broader greenhouse gas mitigation strategies will be indispensable for optimizing future wind-energy resources and ensuring regional climate resilience.

https://doi.org/10.5194/egusphere-2026-1947
Preprint. Discussion started: 27 April 2026

Code availability

The analysis was conducted using Python, and the code used to support the findings of this study is available from the corresponding author upon reasonable request.

Data availability

All data used in this study is publicly available. The CMIP6 and LUMIP model outputs used in this study are publicly available through the Earth System Grid Federation (ESGF; https://esgf-node.llnl.gov/). The CN05.1 observational dataset is available from (Wu & Gao, 2013). The Land-Use Harmonization version 2 (LUH2) dataset is available from the LUH2 project website (https://luh.umd.edu).

Author contributions

Hui-Shuang Yuan and Cheng Shen designed the study. Hui-Shuang Yuan performed the analysis and prepared the first draft. Zi-Han Wang, Zhi-Bo Li, Yang Xu, Zhi-Da Sun, Weiyi Sun, and Youli Chang contributed to the interpretation of the results and revised the manuscript. All authors discussed the results and approved the final version of the paper.

Competing interests

The authors declare that they have no conflict of interest.

Acknowledgements

We acknowledge Python and the open-source community for the quiet efficiency behind our analysis.

Financial support

This work is supported by the Formas (2023-01648), Stiftelsen Längmanska kulturfonden (BA24-0484), Stiftelsen Åforsk (24-707), Herbert & Karin Jacobssons Stiftelse (2025-465), and Adlerbertska Forskningsstiftelsen (AF2024-0069). Zi-Han Wang is supported by the Innovation and Entrepreneurship Training Program for College Students of Yunnan University (S202307019).

https://doi.org/10.5194/egusphere-2026-1947
Preprint. Discussion started: 27 April 2026

References

Bring, J. (1994). How to standardize regression coefficients, *Am. Stat.*, *48*(3), 209-213. https://doi.org/10.1080/00031305.1994.10476059.

Chini, L., G. Hurtt, R. Sahajpal, S. Frolking, K. Klein Goldewijk, S. Sitch, R. Ganzenmüller, L. Ma, et al. (2021). Land-use harmonization datasets for annual global carbon budgets, *Earth Syst. Sci. Data*, *13*(8), 4175-4189. https://doi.org/10.5194/essd-13-4175-2021.

Christidis, N., P. A. Stott, G. C. Hegerl, and R. A. Betts (2013). The role of land use change in the recent warming of daily extreme temperatures, *Geophysical Research Letters*, *40*(3), 589-594. https://doi.org/10.1002/grl.50159.

Chuan, T., J. Wu, J. Zha, D. Zhao, C. Shen, W. Fan, and H. Jiang (2024). Asynchronous changes in terrestrial near-surface wind speed among regions across China from 1973 to 2017, *Atmospheric Research*, *300*. https://doi.org/10.1016/j.atmosres.2024.107220.

Dunn, R. J. H., C. Azorin-Molina, M. J. Menne, Z. Zeng, N. W. Casey, and C. Shen (2022). Reduction in reversal of global stilling arising from correction to encoding of calm periods, *Environmental Research Communications*, *4*(6). https://doi.org/10.1088/2515-7620/ac770a.

Grömping, U. (2007). Relative importance for linear regression in R: the package relaimpo, *J STAT SOFTW*, *17*, 1-27. https://doi.org/10.18637/jss.v017.i01.

Hoerl, A. E., and R. W. Kennard (1970). Ridge regression: Biased estimation for nonorthogonal problems, *Technometrics*, *12*(1), 55-67. https://doi.org/10.1080/00401706.1970.10488634.

Hurtt, G. C., L. Chini, R. Sahajpal, S. Frolking, B. L. Bodirsky, K. Calvin, J. C. Doelman, J. Fisk, et al. (2020). Harmonization of global land use change and management for the period 850–2100 (LUH2) for CMIP6, *Geoscientific Model Development*, *13*(11), 5425-5464. https://doi.org/10.5194/gmd-13-5425-2020.

Ito, A., and T. Hajima (2020). Biogeophysical and biogeochemical impacts of land-use change simulated by MIROC-ES2L, *Prog. Earth Planet. Sci.*, *7*(1), 54. https://doi.org/10.1186/s40645-020-00372-w.

Lawrence, D. M., G. C. Hurtt, A. Arneth, V. Brovkin, K. V. Calvin, A. D. Jones, C. D. Jones, P. J. Lawrence, et al. (2016). The Land Use Model Intercomparison Project (LUMIP) contribution to CMIP6: rationale and experimental design, *Geoscientific Model Development*, *9*(9), 2973-2998. https://doi.org/10.5194/gmd-9-2973-2016.

Li, Y., Y. Wang, H. Chu, and J. Tang (2008). The climate influence of anthropogenic land-use changes on near-surface wind energy potential in China, *Chin. Sci. Bull.*, *53*(18), 2859-2866. https://doi.org/10.1007/s11434-008-0360-z.

Li, Z.-B., Y. Xu, H.-S. Yuan, Y. Chang, and C. Shen (2024). AMO footprint of the recent near-surface wind speed change over China, *Environmental Research Letters*, *19*(11). https://doi.org/10.1088/1748-9326/ad7ee4.

Li, Z., L. Song, H. Ma, J. Xiao, K. Wang, and L. Chen (2017). Observed surface wind speed declining induced by urbanization in East China, *Climate Dynamics*, *50*(3-4), 735-749. https://doi.org/10.1007/s00382-017-3637-6.

https://doi.org/10.5194/egusphere-2026-1947
Preprint. Discussion started: 27 April 2026

Li, Z. B., M. Sun, C. Shen, and D. Chen (2025). ENSO-Driven Seasonal Variability in Near-Surface Wind Speed and Wind Power Potential Across China, *Geophysical Research Letters*, *52*(9). https://doi.org/10.1029/2025gl115537.

Liu, Y., L. Zhou, Y. Qin, C. Azorin-Molina, C. Shen, R. Xu, and Z. Zeng (2024). Impacts of anemometer changes, site relocations and processing methods on wind speed trends in China, *Atmos. Meas. Tech.*, *17*(3), 1123-1131. https://doi.org/10.5194/amt-17-1123-2024.

Long, Y., C. Xu, F. Liu, Y. Liu, and G. Yin (2021). Evaluation and projection of wind speed in the arid region of northwest China based on CMIP6, *Remote Sens-Basel*, *13*(20), 4076. https://doi.org/10.3390/rs13204076.

Minola, L., G. Zhang, T. Ou, J. Kukulies, J. Curio, J. A. Guijarro, K. Deng, C. Azorin-Molina, et al. (2023). Climatology of near-surface wind speed from observational, reanalysis and high-resolution regional climate model data over the Tibetan Plateau, *Climate Dynamics*, *62*(2), 933-953. https://doi.org/10.1007/s00382-023-06931-3.

O'Neill, B. C., C. Tebaldi, D. P. Van Vuuren, V. Eyring, P. Friedlingstein, G. Hurtt, R. Knutti, E. Kriegler, et al. (2016). The scenario model intercomparison project (ScenarioMIP) for CMIP6, *Geosci. Model Dev.*, *9*(9), 3461-3482. https://doi.org/10.5194/gmd-9-3461-2016.

Popp, A., K. Calvin, S. Fujimori, P. Havlik, F. Humpenöder, E. Stehfest, B. L. Bodirsky, J. P. Dietrich, et al. (2017). Land-use futures in the shared socio-economic pathways, *GLOBAL ENVIRON CHANG*, *42*, 331-345. https://doi.org/10.1016/j.gloenvcha.2016.10.002.

Pryor, S. C., and R. J. Barthelmie (2021). A global assessment of extreme wind speeds for wind energy applications, *Nature Energy*, *6*(3), 268-276. https://doi.org/10.1038/s41560-020-00773-7.

Santos, J. F., U. Schickhoff, S. ul Hasson, and J. Böhner (2023). Biogeophysical Effects of Land-Use and Land-Cover Changes in South Asia: An Analysis of CMIP6 Models, *Land*, *12*(4), 880. https://doi.org/10.3390/land12040880.

Shen, C., J. Zha, J. Wu, and D. Zhao (2021). Centennial-scale variability of terrestrial near-surface wind speed over China from reanalysis, *Journal of Climate*, 1-52. https://doi.org/10.1175/JCLI-D-20-0436.1.

Shen, C., J. Zha, Z. Li, C. Azorin-Molina, K. Deng, L. Minola, and D. Chen (2022). Evaluation of global terrestrial near-surface wind speed simulated by CMIP6 models and their future projections, *Ann N Y Acad Sci*, *1518*(1), 249-263. https://doi.org/10.1111/nyas.14910.

Shen, C., J. Zha, J. Wu, D. Zhao, C. Azorin-Molina, W. Fan, and Y. Yu (2022). Does CRA-40 outperform other reanalysis products in evaluating near-surface wind speed changes over China?, *Atmospheric Research*, *266*. https://doi.org/10.1016/j.atmosres.2021.105948.

Shen, C., Z. B. Li, H. S. Yuan, Y. Yu, Y. Lei, and D. Chen (2024). Increases of Offshore Wind Potential in a Warming World, *Geophysical Research Letters*, *51*(14). https://doi.org/10.1029/2024gl109494.

Sierra, J. P., C. Junquas, J. C. Espinoza, H. Segura, T. Condom, M. Andrade, J. Molina-Carpio, L. Ticona, et al. (2021). Deforestation impacts on Amazon-Andes hydroclimatic connectivity, *Climate Dynamics*, *58*(9-10), 2609-2636. https://doi.org/10.1007/s00382-021-06025-y.

https://doi.org/10.5194/egusphere-2026-1947
Preprint. Discussion started: 27 April 2026

Tang, T., X. Lee, K. Zhang, L. Cai, D. M. Lawrence, and E. Shevliakova (2023). Biophysical impact of land-use and land-cover change on subgrid temperature in CMIP6 models, *J. Hydrometeorol.*, *24*(3), 373-388. https://doi.org/10.1175/JHM-D-22-0073.1.

Tebaldi, C., and R. Knutti (2007). The use of the multi-model ensemble in probabilistic climate projections, *Philosophical transactions of the royal society A: mathematical, physical and engineering sciences*, *365*(1857), 2053-2075. https://doi.org/10.1098/rsta.2007.2076.

Tran, D. X., F. Pla, P. Latorre-Carmona, S. W. Myint, M. Caetano, and H. V. Kieu (2017). Characterizing the relationship between land use land cover change and land surface temperature, *ISPRS Journal of Photogrammetry and Remote Sensing*, *124*, 119-132. https://doi.org/10.1016/j.isprsjprs.2017.01.001.

Vautard, R., J. Cattiaux, P. Yiou, J.-N. Thépaut, and P. Ciais (2010). Northern Hemisphere atmospheric stilling partly attributed to an increase in surface roughness, *Nature Geoscience*, *3*(11), 756-761. https://doi.org/10.1038/ngeo979.

Wang, J., J. Feng, Z. Yan, Y. Qiu, and L. Cao (2020). An analysis of the urbanization contribution to observed terrestrial stilling in the Beijing–Tianjin–Hebei region of China, *Environmental Research Letters*, *15*(3), 034062. https://doi.org/10.1088/1748-9326/ab7396.

Wang, J., K. Yang, L. Yuan, J. Liu, Z. Peng, Z. Ren, and X. Zhou (2024). Deducing Aerodynamic Roughness Length From Abundant Anemometer Tower Data to Inform Wind Resource Modeling, *Geophysical Research Letters*, *51*(21). https://doi.org/10.1029/2024gl111056.

Wang, J., K. Yang, J. Liu, X. Zhou, X. Ma, W. Tang, L. Yuan, and Z. Ren (2025). Improvement of near-surface wind speed modeling through refined aerodynamic roughness length in high-roughness surface regions: implementation and validation in the Weather Research and Forecasting (WRF) model version 4.0, *Geoscientific Model Development*, *18*(24), 10077-10094. https://doi.org/10.5194/gmd-18-10077-2025.

Wu, H., C. Fu, L. Zhang, Z. A. Mekonnen, Q. Zhu, K. Yu, P. Ciais, J. Chen, et al. (2025). Significant sensitivity of global vegetation productivity to terrestrial surface wind speed changes, *Nat Commun*, *16*(1), 9315. https://doi.org/10.1038/s41467-025-65000-x.

Wu, J., and X. Gao (2013). A gridded daily observation dataset over China region and comparison with the other datasets, *CHINESE J GEOPHYS-CH (in Chinese)*, *56(4)*(1102-1111). https://doi.org/10.6038/cjg20130406.

Wu, J., X. Gao, F. Giorgi, and D. Chen (2017). Changes of effective temperature and cold/hot days in late decades over China based on a high resolution gridded observation dataset, *Int. J. Climatol.*, *37*, 788-800. https://doi.org/10.1002/joc.5038.

Yan, Y., J. Wu, Q. Chao, and Y. Sun (2026). Overestimation of the recent observed near-surface wind speed recovery in China, *npj Climate and Atmospheric Science*, *9*(1). https://doi.org/10.1038/s41612-026-01322-x.

Yang, Q., M. Li, Z. Zu, and Z. Ma (2021). Has the stilling of the surface wind speed ended in China?, *Science China Earth Sciences*, *64*(7). https://doi.org/10.1007/s11430-020-9738-4.

Yuan, H.-S., J. Piao, Y. Chang, and C. Shen (2025). Simulated and projected near-surface wind speed in High-Resolution Model Intercomparison Project, *Climate Dynamics*, *63*(8). https://doi.org/10.1007/s00382-025-07792-8.

https://doi.org/10.5194/egusphere-2026-1947
Preprint. Discussion started: 27 April 2026

Zeng, Z., A. D. Ziegler, T. Searchinger, L. Yang, A. Chen, K. Ju, S. Piao, L. Z. X. Li, et al. (2019). A reversal in global terrestrial stilling and its implications for wind energy production, *Nature Climate Change*, *9*(12), 979-985. https://doi.org/10.1038/s41558-019-0622-6.

Zha, J., J. Wu, and D. Zhao (2016). Effects of land use and cover change on the near-surface wind speed over China in the last 30 years, *Progress in Physical Geography: Earth and Environment*, *41*(1), 46-67. https://doi.org/10.1177/0309133316663097.

Zha, J., C. Shen, Z. Li, J. Wu, D. Zhao, W. Fan, M. Sun, C. Azorin-Molina, et al. (2021a). Projected changes in global terrestrial near-surface wind speed in 1.5 C–4.0 C global warming levels, *Environmental Research Letters*, *16*(11), 114016. https://doi.org/10.1088/1748-9326/ac2fdd.

Zha, J., C. Shen, D. Zhao, J. Wu, and W. Fan (2021b). Slowdown and reversal of terrestrial near-surface wind speed and its future changes over eastern China, *Environmental Research Letters*, *16*(3). https://doi.org/10.1088/1748-9326/abe2cd.

Zha, J., D. Zhao, J. Wu, and C. Shen (2021c). Terrestrial Near-Surface Wind Speed Variations in China: Research Progress and Prospects, *Journal of Meteorological Research*, *35*(3), 537-556. https://doi.org/10.1007/s13351-021-0143-x.

Zha, J., T. Chuan, J. Wu, D. Zhao, M. Luo, J. Feng, W. Fan, C. Shen, et al. (2024). Attribution of Terrestrial Near-Surface Wind Speed Changes Across China at a Centennial Scale, *Geophysical Research Letters*, *51*(7). https://doi.org/10.1029/2024gl108241.

Zhang, Z., K. Wang, D. Chen, J. Li, and R. Dickinson (2019). Increase in Surface Friction Dominates the Observed Surface Wind Speed Decline during 1973-2014 in the Northern Hemisphere Lands, *Journal of Climate*, *32*(21), 7421-7435. https://doi.org/10.1175/jcli-d-18-0691.1.

Zhang, Z., J. Xu, Y. Zhang, H. Zhuang, S. Li, F. Tao, and Z. Zhang (2025). Decadal changes in wind speed have offset and then aggravated the impact of warming on maize production in China since 1980, *Nat Commun*, *16*(1), 9739. https://doi.org/10.1038/s41467-025-64725-z.

Zheng, C. W., J. Pan, and C. Y. Li (2016). Global oceanic wind speed trends, *Ocean & Coastal Management*, *129*, 15-24. https://doi.org/10.1016/j.ocecoaman.2016.05.001.